Decadal Variability of the Indo-Pacific Warm Pool and Its Association with Atmospheric and Oceanic Variability in the NCEP–NCAR and SODA Reanalyses

HUI WANG* AND VIKRAM M. MEHTA

The Center for Research on the Changing Earth System, Columbia, Maryland

(Manuscript received 17 May 2007, in final form 29 January 2008)

ABSTRACT

Decadal variability of the Indo-Pacific warm pool (IPWP) sea surface temperature (SST) and its association with atmospheric and oceanic circulations are investigated with observed 50-yr (1952–2001) SST, and the NCEP–NCAR atmospheric and Simple Ocean Data Assimilation (SODA) oceanic reanalysis data. The decadal variability of the IPWP SSTs was analyzed by applying an empirical orthogonal function technique to low-pass-filtered SSTs. Two leading empirical modes (EMs) well represent the IPWP SST decadal variations. EM1 is an ENSO-like pattern with out-of-phase SST anomalies in the western Pacific and the Indian Ocean, whereas EM2 displays an in-phase relationship between SST anomalies in the two regions. Consequently, spatial evolution of EM1 is dominated by opposing changes in zonal and meridional dimensions and thus a strong deformation of the warm pool on decadal time scales. EM2 is dominated by changes in size and intensity of the warm pool.

Analyses of ocean thermodynamic fields associated with the two SST EMs indicate that decadal changes in the IPWP can extend down to 300-m depth. Oceanic processes may thus be involved in the IPWP decadal variability, including advections of mean temperature by both mean and anomalous ocean currents and effects of shallow tropical circulations (STCs) on the IPWP SST, which is consistent with some previous studies on tropical decadal variability. The results may also indicate the existence of both positive and negative feedbacks between the IPWP SST and the STCs.

Both December–January–February (DJF) and June–July–August (JJA) atmospheric circulations exhibit thermally direct responses to the two decadal IPWP SST EMs by altering the Hadley and Walker circulations. In addition, significant upper-level rotational flow anomalies in the extratropics are found to be associated with the decadal IPWP SST variability. Consistent with the upper-level flow anomalies and 850-hPa convergence–divergence patterns associated with the two SST EMs are rainfall anomalies over the United States. In DJF, the rainfall anomalies are mainly in Florida, the Gulf Coast, southern Texas, Arizona, and along the West Coast. In JJA, the rainfall anomalies are mainly in the Midwest and the Southeast. Since these rainfall anomalies are a significant fraction of seasonal-average rainfall and since these anomalies persist for many years, they potentially make a significant impact on U.S. water resources and agriculture. Further analysis of observations and modeling studies are required to understand the physics of the IPWP SST decadal variability and its impacts on global climate, and to assess its predictability.

1. Introduction

The Indo-Pacific warm pool (IPWP) contains some of the warmest ocean water in the world. Its formation is fundamentally driven by ocean dynamics, but atmospheric processes also play an important role (Ramanathan and Collins 1991; Waliser and Graham 1993; Ramanathan et al. 1995; Schneider et al. 1996; Clement et al. 2005). The IPWP is characterized by persistently warm sea surface temperature (SST) higher than 28°C, which is a threshold for atmospheric deep convection (e.g., Fu et al. 1994). Since saturation vapor pressure is an exponential function of SST (Graham and Barnett 1987; Fu et al. 1994), the intensity of deep convection is very sensitive to changes in SST over the warm pool region. Even small changes in IPWP SST can cause large changes in atmospheric convection, which in turn can dramatically alter atmospheric divergent flow locally, and further significantly modify planetary-scale

* Current affiliation: Wyle Information Systems, and NOAA/Climate Prediction Center, Camp Springs, Maryland.

Corresponding author address: Vikram M. Mehta, The Center for Research on the Changing Earth System, 10211 Wincopin Circle, Suite 240, Columbia, MD 21044.
E-mail: Vikram@crces.org

DOI: 10.1175/2008JCLI2049.1

wave activity and atmospheric heating globally (Sardeshmukh and Hoskins 1988; Neale and Slingo 2003). The IPWP is also a region of net 1–2 m yr^{-1} atmospheric freshwater input to the ocean (Chen et al. 2004; Huang and Mehta 2004). This mass and buoyancy flux significantly affects the dynamics and thermodynamics of the IPWP via its effect on salinity and ocean–atmosphere heat flux (Lindstrom et al. 1987; Godfrey and Lindstrom 1989; Lukas and Lindstrom 1991; Huang and Mehta 2004, 2005). The IPWP is thus an important source of energy for driving atmospheric circulation, an important sink of atmospheric freshwater, and constitutes an important component of the global climate system.

The IPWP exhibits large variations in area on intraseasonal to decadal time scales. Its spatial coverage (SST $>$ 28°C) may vary as much as 25%, 22%, and 11%, respectively, on seasonal, interannual, and decadal time scales, with respect to its climatology. These variations influence both mean and anomalous atmospheric circulations and also interact with a number of important weather–climate systems, including the Madden–Julian oscillation (MJO), the El Niño–Southern Oscillation (ENSO), and the Asian monsoon (e.g., Fasullo and Webster 1999; Matsuura and Iizuka 2000; Tian et al. 2001; D'Arrigo et al. 2006). For example, Wang and Xie (1998) demonstrated that the mean state of warm SST in the IPWP favors atmosphere–ocean coupled unstable modes on the intraseasonal time scale and thereby sustains the MJO. On the interannual time scale, the strong east–west migration of the warm pool in the equatorial western Pacific is closely tied to the surface current variation driven by the ENSO-related surface winds (Picaut et al. 1996). Both analytical and modeling studies (Clarke et al. 2000; Solomon and Jin 2005) indicate that the interannual variability of SST over the western Pacific warm pool has a positive feedback to the ENSO cycle.

The decadal variability of the IPWP has not received much attention until recent years. Analyses of coral-based proxy records show significant and consistent decadal to multidecadal thermal and hydrologic variations in the IPWP region, which correlate with the ENSO and Asian monsoon in decadal frequency bands (D'Arrigo et al. 2006; Brijker et al. 2007). The decadal changes in the IPWP SST can be a response to basin-scale heat advection forced by large-scale net atmospheric freshwater flux (Huang and Mehta 2005). Mehta and Fayos (2005), illustrated that the decadal–multidecadal IPWP variability can modulate the interannual variability of ENSO. Significant signals of 850-hPa wind anomaly on a global scale are also found associated with the decadal–multidecadal IPWP SST (Mehta and Mehta 2007, manuscript submitted to *Geophys. Res. Lett.*). These results considerably increase our knowledge of the IPWP decadal variability and its climate impact. In these studies, the IPWP variability was examined by using either oxygen isotopes at isolated spots or area-averaged SST over the whole warm pool domain. The detailed variation of the IPWP on decadal time scales, particularly its spatial evolution, has not been well documented or understood.

Figure 1 shows an example of decadal variation of the IPWP in the 1990s, which is represented by low-pass-filtered ($>$7 yr) annual mean SST anomaly superimposed onto a long-term (1948–2005) climatological annual mean SST derived from the National Oceanic and Atmospheric Administration (NOAA) reconstructed SST data (Smith and Reynolds 2004). The warm pool SST in the 1990s (Figs. 1b,c) was apparently warmer than the long-term mean (Fig. 1a). In the early 1990s, maximum SSTs were confined to the South Pacific convergence zone (SPCZ) between 160°E and 170°W (Fig. 1b), with little change in the shape of the warm pool (SST $>$ 28°C, Figs. 1d–f). In the late 1990s, regions of maximum SST shifted toward the west (Figs. 1c–e). The warmest water piled up to the northeast of New Guinea at the end of the decade, leading to significant zonal withdrawal of its northern branch across the date line (Fig. 1e) and northward extension of the warm pool (Fig. 1f). The observational evidence on the decadal variation of the IPWP SST naturally raises questions as to whether the changes of the warm pool shown in Fig. 1 are representative of the dominant modes of the IPWP decadal variability, and if so, what atmospheric and oceanic processes are related to them.

Several previous studies describe in detail decadal variability in the tropical Pacific with an emphasis on the decadal variation of the ENSO in the eastern and central Pacific (e.g., Trenberth and Hurrell 1994). The origin of the tropical decadal variability is proposed to be in both the tropical Pacific (Graham 1994) and North Pacific (Gu and Philander 1997) through advection of temperature by ocean currents and tropical–extratropical exchanges. An alternative explanation is an influence of shallow tropical/subtropical overturning cells (STCs; McCreary and Lu 1994; Liu 1994) on the tropical Pacific SST decadal variability (Lohmann and Latif 2005; Zhang and McPhaden 2006). Whether those mechanisms are also responsible for the IPWP SST decadal variability is not clear. According to the Fourth Assessment Report of the Intergovernmental Panel on Climate Change (IPCC; Solomon et al. 2007), global temperatures in the last two decades were the highest since 1850. It is also true for both the intensity and size

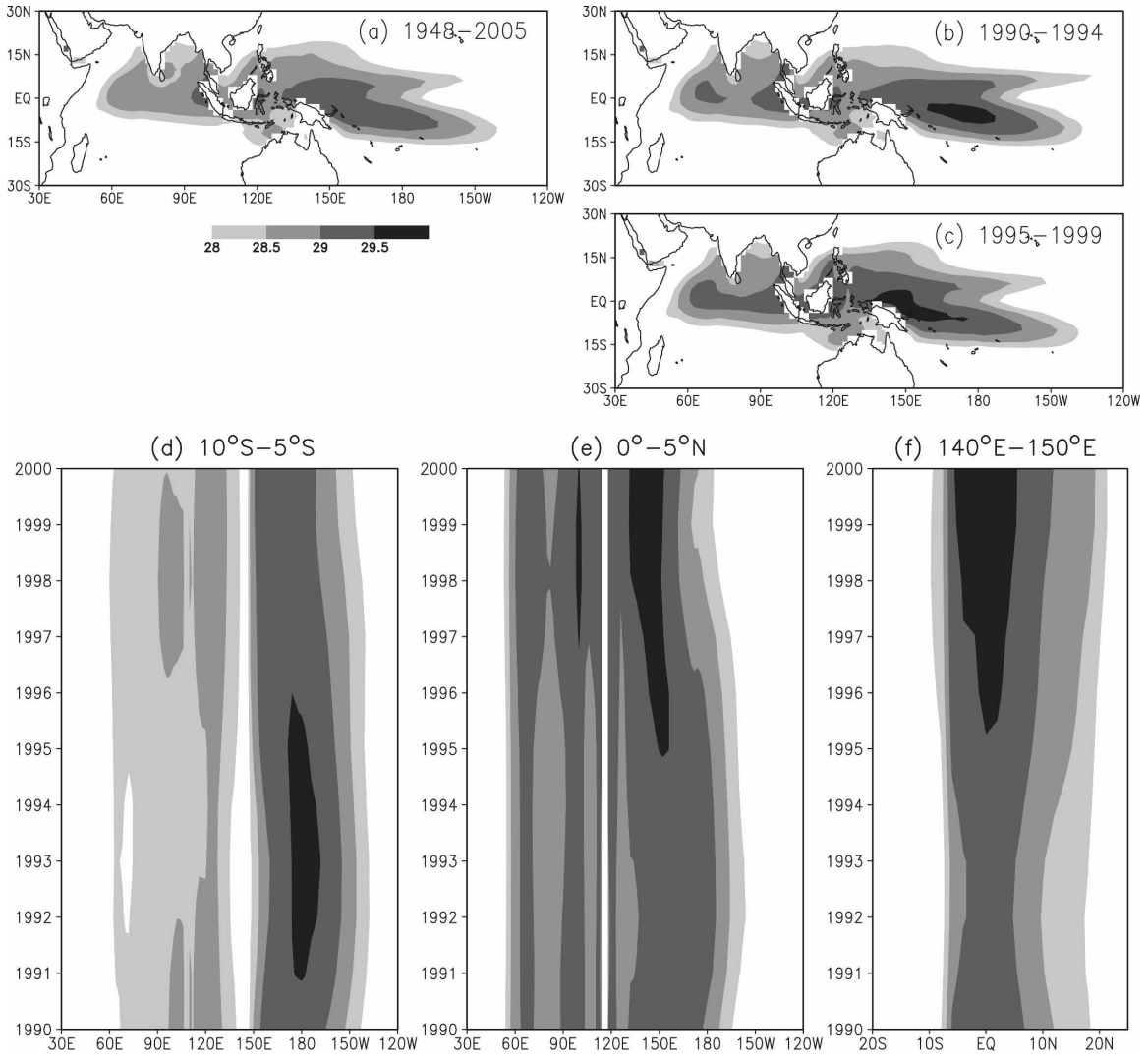

FIG. 1. (a) Long-term (1948–2005) annual mean SST in the IPWP region; 5-yr average annual mean SST during (b) 1990–94 and (c) 1995–99; time–longitude diagram of SST averaged over (d) 10°–5°S and (e) 0°–5°N; and (f) time–latitude diagram of SST averaged over 140°–150°E from 1990 to 1999. The SSTs in (b)–(f) are low-pass-filtered (>7 yr) annual mean anomalies superimposed onto the long-term annual mean SST climatology. Shaded areas indicate SST greater then 28°C; the SST scale is shown below (a).

of the IPWP SST. The decadal-scale warm pool behavior in the 1990s (Fig. 1) apparently differs from that associated with the global warming (Solomon et al. 2007). Therefore, a fundamental question addressed in the present study is whether the decadal variability of the IPWP is spatially homogeneous across the warm pool or it has specific patterns that are independent of the global warming pattern. Understanding this problem is of particular interest if the IPWP decadal variability can be used as a potential predictor for decadal climate predictions. Of interest for this study are also atmospheric and oceanic circulations associated with different IPWP regimes on decadal time scales. In the next section, the datasets and statistical techniques are described. The variability of the IPWP SST and relative importance of the decadal variability versus higher-frequency variability are assessed in section 3. Dominant empirical modes of the IPWP decadal variability are described in section 4. The atmospheric and oceanic circulations related to the IPWP decadal variability are described in sections 5 and 6, respectively. Conclusions are given in section 7.

2. Data and methods

The data used in this study include SST; U.S. rainfall; and three-dimensional atmospheric wind, ocean temperature, and ocean current fields. The SSTs are from the NOAA extended reconstructed SST version 2

dataset (ERSST.v2; Smith and Reynolds 2004) on a 2° longitude–2° latitude grid. Unlike the high-frequency (interannual) component of these SST data, the low-frequency (decadal–interdecadal) component is not reconstructed using empirical functions based on recent SST data, therefore it is not likely that the most recent, dominant, low-frequency spatial patterns emerge from the reconstructed SST data further back in time. Therefore, the robustness of our results based on the 1952–2001 SST data was addressed by performing a similar analysis with the 1902–51 SST data. Although these reconstructed historical SST data are most accurate in the post-1950 period (Smith and Reynolds 2004), results must be interpreted with caution because of sparse spatial and temporal coverage, and unknown accuracy of SST and subsurface ocean observations in the IPWP region before the 1980s.

The atmospheric wind fields are the National Centers for Environmental Prediction–National Center for Atmospheric Research (NCEP–NCAR) reanalysis product (Kalnay et al. 1996) on a 2.5° longitude–2.5° latitude grid. Ocean temperature and current data are from a Simple Ocean Data Assimilation (SODA) reanalysis (Carton et al. 2000) with a spatial coverage of 60°N–60°S, horizontal resolutions of 1° longitude–0.4° latitude at the equator and increasing to 1° latitude at 60° latitude, and 20 vertical levels from 7.5- to 3622-m depth. Both the atmospheric and oceanic reanalysis fields examined in this study cover a 50-yr period from 1952 to 2001.

Although there are no discontinuities related to changes in data assimilation systems and model physics in both the NCEP–NCAR and SODA reanalyses, problems related to discontinuities in spatial and temporal distribution of raw observational data exist (Kistler et al. 2001). Comparisons between the reanalysis data and some independent data sources in previous studies (e.g., Schott et al. 2002; Xie et al. 2002; Chelliah and Bell 2004) indicate that both reanalysis datasets well represent climate variability of atmospheric and ocean circulations in the tropics over the 50-yr period. The NCEP–NCAR reanalyses have also been used to examine tropical decadal variability by Ashok et al. (2002) and Chelliah and Bell (2004). The earlier-mentioned unreliability of pre-1980s ocean observations, however, renders the longer data length of the SODA product problematic. Also, SODA contains internal sources/sinks of heat generated by the assimilation procedure in addition to the usual physical terms in the heat equation. This poses a major difficulty in heat budget analysis using the SODA product (Fukumori, 2006). But, we used the SODA product in this study only for an exploratory purpose as used by Schoenefeldt and Schott (2006) to explore decadal variability of the Indian Ocean circulation.

The U.S. rainfall data are taken from the NOAA/Climate Prediction Center (CPC) U.S. Unified Daily Precipitation Analysis for 1948–98 and from the real-time U.S. Daily Precipitation Analysis for 1999–2005 (Higgins et al. 2000). Both datasets are on a 0.25° longitude–0.25° latitude grid.

We used monthly-average data. Prior to analyses, the 58-yr (1948–2005) SSTs were processed through a Lanczos low-pass filter (>7 yr; Duchon 1979) to eliminate interannual and higher-frequency variability. This procedure reduces the SST data size to 50 yr from 1952 to 2001, which is the focused period of this study. The seasonality of the IPWP decadal variability and associated atmospheric and oceanic circulations are examined by averaging monthly average of December–January–February (DJF) and June–July–August (JJA) for boreal winter and summer, respectively.

Two statistical methods were used to characterize the decadal variability of the IPWP and to analyze its relation to atmospheric and oceanic circulations. One was empirical orthogonal function (EOF) analysis, and the other was linear regression. The former is able to objectively identify dominant patterns of variability if they exist, which is a conventional and effective technique used in many previous studies of decadal variability (e.g., Zhang et al. 1997; Chelliah and Bell 2004; Yeh and Kirtman 2004). The latter was used to create contour maps of anomalous atmospheric and oceanic circulations associated with the IPWP decadal variability. The significance of the statistical results was estimated by the Monte Carlo technique (see, e.g., Wang and Fu 2000). Briefly, in this technique, the statistical significance of anomalies constructed with the linear regression is estimated by the Monte Carlo tests. It is a type of resampling process to create many new data time series with the same size as the original time series by randomly rearranging the temporal order of the original data. Linear regression analyses using these synthetic data time series produce a pool of reference test statistics. If a value calculated using the original data is high enough to fall into the top 1% rank in the reference test statistics, then it is defined to exceed the 1% significance level.

3. Variability of the Indo-Pacific warm pool

To describe the variability of the IPWP, an IPWP index was constructed by averaging SST over the IPWP region (20°S–20°N, 90°E–180°) where SST was equal to or greater than 28°C using unfiltered monthly data of 1948–2005. The 58-yr monthly SST time series, after

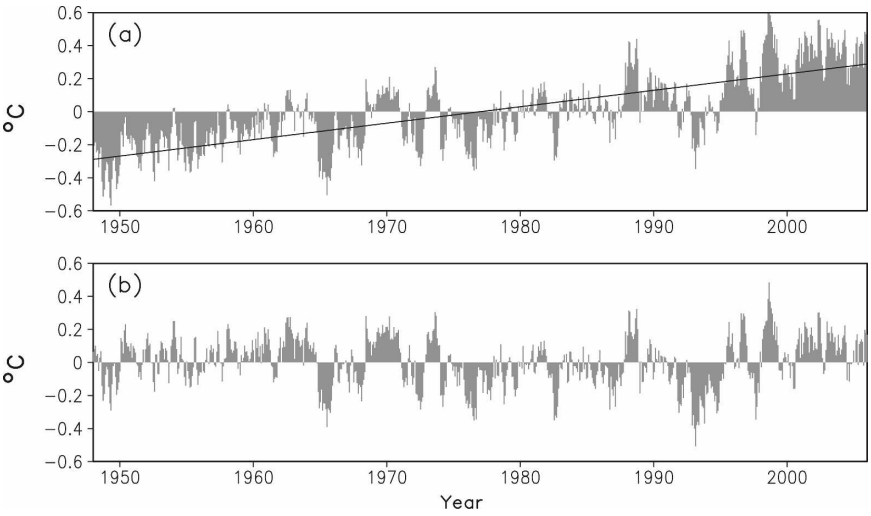

FIG. 2. (a) Time series of monthly mean SST anomaly averaged over the IPWP region (20°S–20°N, 90°E–180°) for 1948–2005 and (b) same time series after removing a warm trend, which is indicated by a straight line in (a).

removing its climatological seasonal cycle, is shown in Fig. 2a. An apparent warming trend indicates a 0.58°C increase in the warm pool SST over the 58 yr, equivalent to a warming rate of 0.1°C decade^{-1}, which is larger than the global SST warming trend (0.07°C decade^{-1}) in the same SST dataset. The detrended IPWP index (Fig. 2b) exhibits large interannual and decadal variations with significant strong peaks at 1.5, 2.1, 3.5, and 9.7 yr in a power spectrum analysis (not shown). The IPWP variability is thus characterized by strong interannual and decadal variations in addition to the warming trend. It is also interesting to note that even with the warming trend removed, there was additional warming of the IPWP SST from cold anomalies during the mid-1970s–mid-1990s to warm anomalies after the mid-1990s (Fig. 2b). The standard deviations of the IPWP SST index associated with the interannual (<7 yr) and decadal variability (>7 yr) are 0.12° and 0.06°C, respectively, suggesting a considerable contribution of decadal SST changes to the total variability of the IPWP SST. The strength of the decadal variability is also comparable to the 0.1°C increase in SST per decade associated with the warming trend. To highlight these decadal SST signals and to exclude variations on the interannual time scales and those associated with the warming trend, the SST data were detrended and low-pass filtered (>7 yr) prior to subsequent analyses.

4. Decadal variability of the Indo-Pacific warm pool

To identify dominant empirical modes (EMs) of the IPWP decadal variability, an EOF analysis was performed using the variance matrix of monthly SST anomalies (1952–2001) within the warm pool region bounded by 25°N–25°S, 60°E–160°W. The results, however, are not sensitive to the exact boundaries of the EOF analysis domain. The first two EMs account for 45% and 18% of the total decadal SST variance over the domain, respectively. They are distinct and well separated from the rest of the EMs based on a "rule of thumb," that is, distinctness of eigenvalues, suggested by North et al. (1982). Figure 3 shows the spatial patterns of the two EMs in the form of regressions of filtered SST anomalies against the time series of corresponding EMs. The EM1 is characterized by large areas of statistically significant SST anomalies at the 1% level; there are warm SST anomalies in the central and eastern equatorial Pacific, cold SST anomalies in the western Pacific, and warm SST anomalies in most of the Indian Ocean (Fig. 3a). It bears some resemblance to the El Niño SST pattern in the tropical Pacific, but with relatively weak and insignificant SST anomalies in the eastern Pacific and a much broader meridional extent. Near the equator, the warmest SST anomalies in the central Pacific and cold SST in the western Pacific set up a strong zonal SST gradient between 150°E and 180°. In the IPWP region, there is an out-of-phase relationship between SST anomalies in the Indian Ocean and the western Pacific. This EM is similar to the ENSO-like decadal mode in Lohmann and Latif (2005), suggesting a linkage between the IPWP and ENSO on decadal time scales. The SST pattern in EM2 shows statistically significant, coherent warm SST anomalies in the IPWP as well as in the tropical Pacific, except for two small areas centered at 180° and 120°W where the

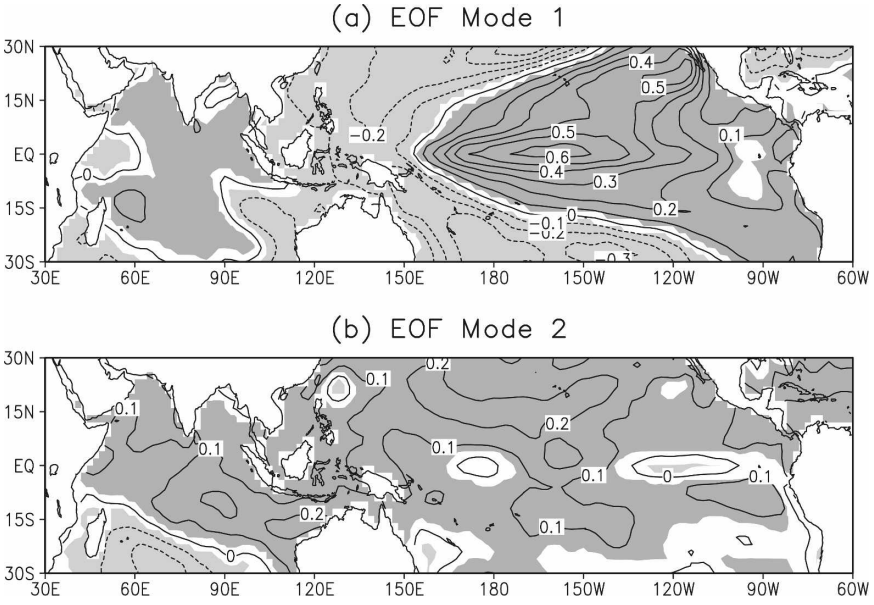

FIG. 3. Regression patterns of SST anomaly (contours) associated with a two standard deviation departure in the corresponding EOF time series. Contour interval is 0.1°C and negative contours are dashed. Dark (light) shadings indicate positive (negative) SST anomaly at the 1% significance level, estimated by Monte Carlo tests.

anomalies are insignificant (Fig. 3b). The normalized time series of the principal components (PCs) corresponding to the two EMs are shown in Figs. 4a,b, respectively. Both time series exhibit apparent decadal variations. Their phase diagram, shown in Fig. 4c, also suggests irregular oscillations on the decadal time scale.

As mentioned in section 2, since the SST data in the IPWP region were relatively sparse in the pre-1980s period, the robustness of the two EMs are tested by a similar EOF analysis on low-pass filtered and detrended 50-yr SST data in the pre-1952 (1902–51) period. The spatial patterns of the two EMs in the pre-

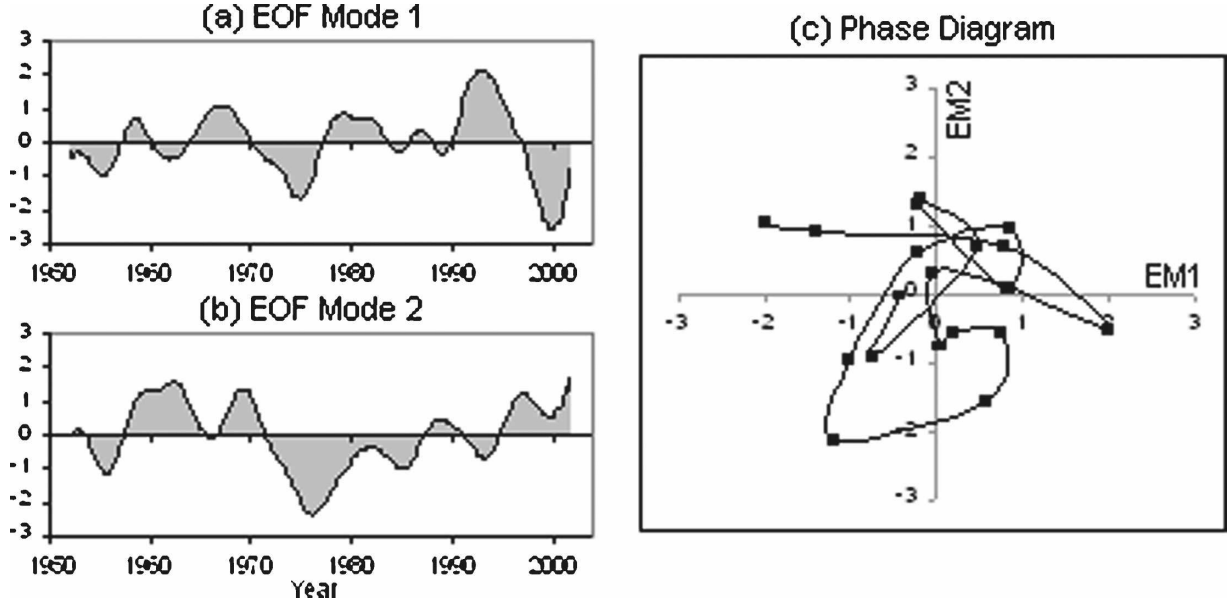

FIG. 4. Normalized monthly time series (1952–2001) of (a) EM1 and (b) EM2 of the IPWP SST, and (c) phase diagram of EM1 and EM2 with 2.5-yr averages of each time series.

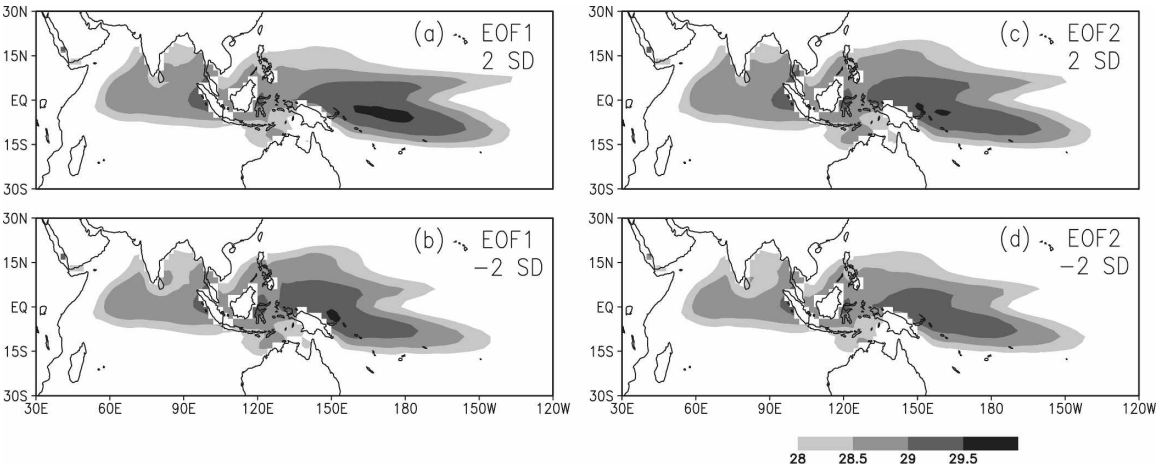

FIG. 5. Reconstructed SST associated with (a),(c) positive and (b),(d) negative two standard deviation (2 SD) departure in the time series of (a),(b) the first and (c),(d) second EOF modes. Shaded areas indicate SST greater then 28°C.

1952 period are similar to those in the post-1952 period (Fig. 3), with pattern correlations of 0.77 and 0.71, respectively, between corresponding modes. This suggests that the two EMs remain robust in the pre- and post-1952 periods. This similarity of pre- and post-1952 EM patterns is not likely to have been produced by the SST data reconstruction technique (Smith and Reynolds 2004).

To assess how the decadal variation of the IPWP SSTs, shown in Fig. 1, is related to the two EMs, Fig. 5 shows reconstructed total SST based on regressions of low-pass-filtered SST anomalies versus the time series of each EM and long-term annual-average SST climatology. Associated with a two standard deviation fluctuation in a positive phase of EM1, that is, positive values in the time series of Fig. 4a, the IPWP shows a zonal band of warmest SST (>29.5°C) to the south of the equator between 160°E and 170°W, with its northern branch (>28°C) reaching 135°W (Fig. 5a). As the SST anomalies associated with EM1 shift from the positive phase to the negative phase, significant zonal changes of the warm pool occur in the western and central Pacific, and also significant meridional extension occurs near 150°E (Fig. 5b). The warmest SSTs (>29.5°C) migrate westward to 150°E. The northern branch of the warm pool also retreats westward. These zonal variations of the warm pool are consistent with the negative phase of EM1 (Fig. 3a), with warmer SST anomalies in the western Pacific and colder SST to the east. Differences in the IPWP associated with EM2 between positive and negative phases are mainly changes in intensity (or size) of SST (Figs. 5c,d), with little change in the shape of the warm pool. This is consistent with the homogeneity of SST anomalies across the Indian Ocean and the tropical Pacific in this EM (Fig. 3b). Figure 5 suggests that each EM describes one aspect of the IPWP decadal variability. EM1 mainly represents zonal and meridional spatial variations of the warm pool in the central and western Pacific, whereas EM2 represents changes in intensity of the warm pool temperature.

Combinations of different phases and amplitudes of the two EMs based on their respective PC time series (Fig. 4) can reproduce very well the decadal variation of the IPWP observed in the 1990s (not shown). In the first half of the 1990s, Fig. 4 shows a strong positive phase of EM1 but a weak negative phase of EM2. The decadal variation of the IPWP in the early 1990s (Fig. 1) is thus dominated by EM1 and displays a persistent pattern similar to that in Fig. 5a. In the late 1990s, both EMs change their phase with larger amplitudes (Fig. 4). Therefore, in addition to the dominance of EM1 (Fig. 5b) in the westward shift of the warmest SST and northern branch of the warm pool, EM2 (Fig. 5c) also contributes considerably to the maximum SST to the northeast of New Guinea in the late 1990s (Fig. 1). Both EMs account for the strong northward expansion of the warm pool in the subtropics. The results indicate that the decadal variation of the IPWP in the 1990s is indeed a manifestation of the dominant EMs of the decadal variability. In the IPWP region (20°S–20°N, 90°E–180°) SST on average was increased by 0.38°C from 1990 to 1999 (Fig. 2a). The long-term linear trend (0.1°C decade^{-1}) shown in Fig. 2a only contributed to 26% of the total IPWP SST warming. In contrast, the decadal variations of EM1 and EM2 caused 0.13° and 0.09°C increase in IPWP SST, respectively. Together the two modes account for 58% of the warming. Therefore, the

IPWP SST warming in the 1990s (Fig. 2a) was largely contributed by the two EMs and less related to the global warming linear trend.

5. Atmospheric circulation variability associated with the IPWP decadal variability

As described in the introduction, warm SSTs in the IPWP activate tropical deep convection and may contribute to thermally direct Hadley and Walker circulations. Associations between decadal variability of the IPWP SSTs and variability in these thermally direct circulations were examined by constructing mean meridional and zonal flows based on linear regressions versus the two PC time series (Fig. 4). Figure 6 shows the Hadley circulation and anomalous vertical velocity field associated with the positive phase of the two EMs for DJF and JJA, respectively, which are the averages of meridional divergent flow and vertical velocity across the warm pool between 60°E and 160°W. Please note that the negative of vertical velocity in pressure coordinates is plotted so that it is consistent with circulations (positive upward). In DJF (Figs. 6a,b, top panel) the Hadley circulation is characterized by low-level convergence, upper-level divergence, and strong updrafts in the middle troposphere between 20°S and 10°N, and downdrafts at higher latitudes. The circulation associated with the negative phase of the two EMs (not shown) also has this seasonal feature. A close inspection, however, suggests that the two EMs modulate the mean meridional circulation in different ways. The anomalous vertical velocity related to the two EMs (Figs. 6a,b, bottom panel) indicates that in their positive phase both EMs contribute to the upward motion near the equator. EM1 has much stronger and broader impact than EM2. Additionally, in the northern extratropics the descending branch is greatly enhanced by EM1, but weakened by EM2. This is consistent with the spatial distribution of SST shown in Fig. 3, in which cold SST anomalies dominate most of the northern extratropics in EM1, while in EM2 there are warm SST anomalies in the same region. In the Southern Hemisphere, both EMs weaken the meridional circulation by reducing ascending motion in the subtropics and increasing subsidence in midlatitudes. In general, the contrasts in the Southern Hemisphere between the two EMs are smaller than those in the tropics and the Northern Hemisphere. In JJA (Figs. 6c,d), both low-level convergence and upper-level divergence, as well as the tropical updrafts, shift into the Northern Hemisphere, consistent with northward movement of the northern branch of the IPWP (not shown). The downdrafts in the Southern Hemisphere are much stronger in JJA than in DJF. The anomalous vertical velocity associated with EM1 in its positive phase enhances the Hadley circulation in the tropics in JJA. In contrast, the anomalous vertical velocity related to EM2 in JJA only strengthens the Hadley circulation between 10°S and the equator, but weakens the Hadley circulation between 30°N and the equator.

Similar analyses are shown in Fig. 7 for the Walker circulation, that is, averages of zonal divergent flow and vertical velocity between 2.5°S and 2.5°N. In the Walker circulation, low-level cold and dry air from the tropical eastern Pacific flows westward to the IPWP where the air is heated and moistened. After moist-adiabatic ascent and rainfall over the IPWP, the upper-level outflow moves eastward, and converges and subsides over the tropical eastern Pacific. The two IPWP decadal EMs exhibit clear associations with the Walker circulation. In both DJF and JJA (Figs. 7a,c), anomalous circulation related to the positive phase of EM1 reinforces the updrafts in the central Pacific and Indian Ocean but reduces the ascent over the western Pacific, resulting from a thermally direct response to the anomalous SSTs in Fig. 3a. The anomalous vertical velocity associated with EM2 (Figs. 7b,d) is weaker than that associated with EM1 in both seasons, possibly because anomalous zonal SST gradient is much stronger in EM1 than in EM2. In the western Pacific, EM2 strengthens the Walker circulation, which is opposite to the effect of EM1 and consistent with warm SST anomalies in EM2 in the same region (Fig. 3b). It is noted that both EMs in their positive phase weaken ascending motion over equatorial South America.

Figure 8 presents anomalous components of the Hadley and Walker circulations associated with the two EMs. As Figs. 8a–d show, the modulation of the thermally direct Hadley circulations by the two decadal EMs has strong seasonality. The statistically significant contribution of EM1 is slightly stronger and encompasses a larger atmospheric column in DJF but is comparable to that in JJA with a northward shift, whereas the statistically significant contribution of EM2 to the Hadley circulation in DJF is much weaker than that in JJA. The influence of EM2 is also stronger in the Northern Hemisphere than in the Southern Hemisphere. It is interesting to note that while the circulation anomalies in the rising branch of the Hadley circulation in DJF (Fig. 8a) are significant only in the lower troposphere near the equator, circulation anomalies in the descending branches are significant over almost the entire troposphere in both Hemispheres.

The anomalous Walker circulation associated with

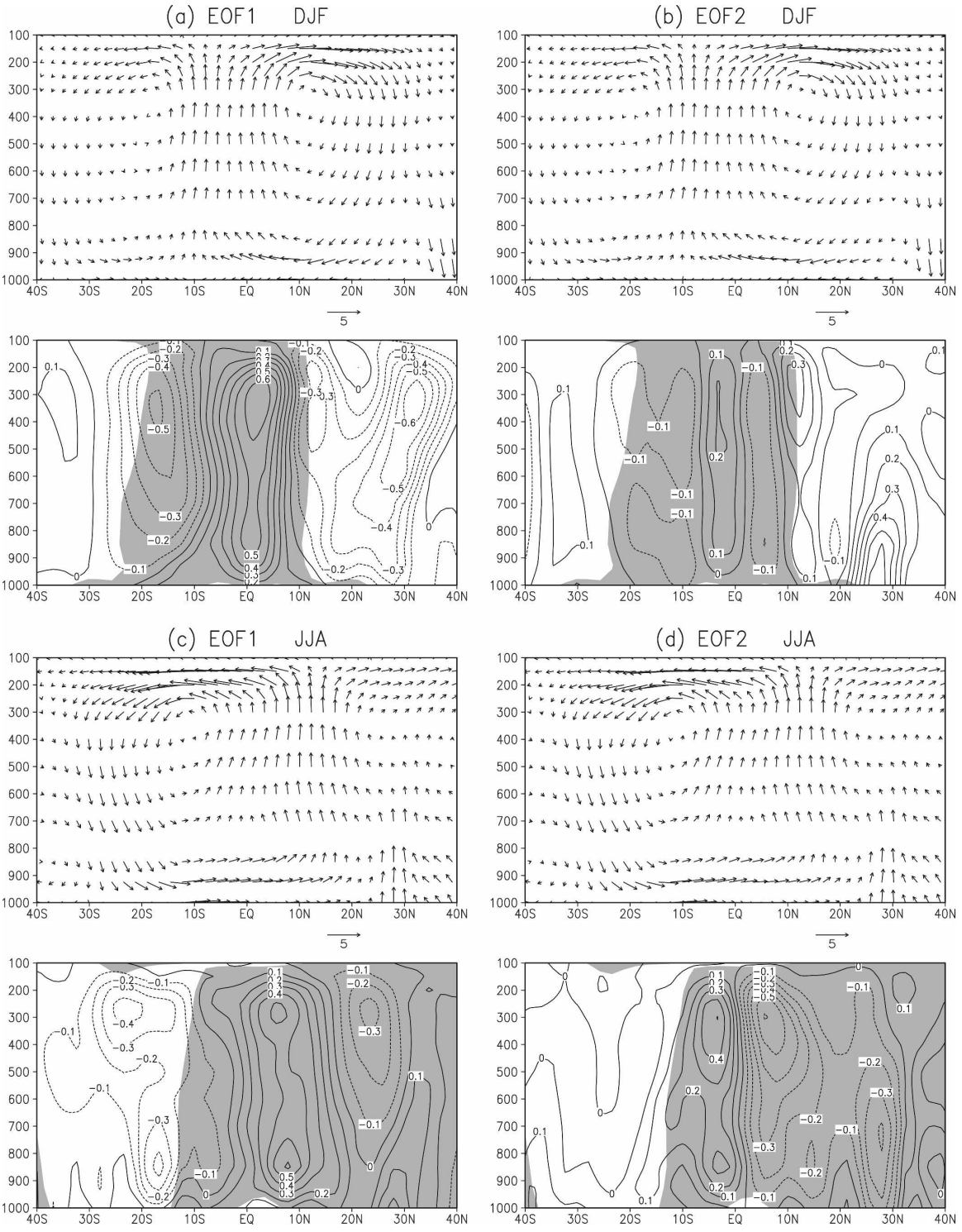

FIG. 6. (top) Total Hadley circulation (vectors) and (bottom) the negative of anomalous vertical velocity (contours) for (a),(b) DJF and (c),(d) JJA associated with the two leading EOFs of IPWP SST, respectively. The maps are linear regressions vs each EOF time series and averaged between 60°E and 160°W. The vertical velocity anomaly is the difference between the regressions associated with positive and negative EOF phases. Contour interval is 0.1 with a unit of -0.02 Pa s^{-1} and negative contours are dashed. Shadings indicate updrafts in climatological seasonal mean circulation.

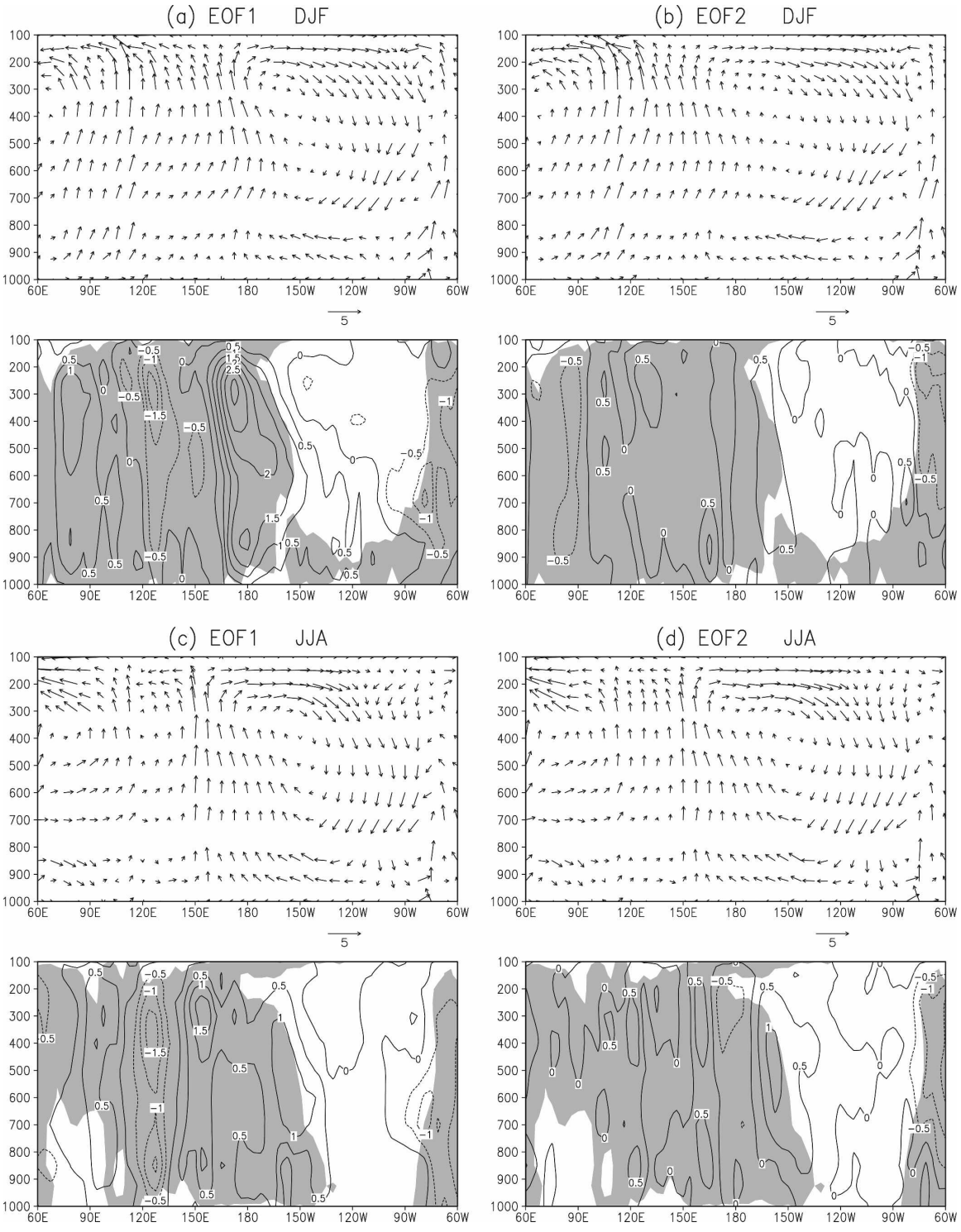

FIG. 7. As in Fig. 6, but for Walker circulation averaged between 2.5°S and 2.5°N.

EM1 (Fig. 8e) is large and statistically significant. This is physically consistent with the large zonal gradient of SST anomalies in EM1 (Fig. 3a) near the equator. In both DJF (Fig. 8e) and JJA (Fig. 8g), the rising branch of the anomalous Walker circulation associated with EM1 is near 180° because the warmest SST anomalies are near 180°. In contrast, the anomalous Walker circulations (Figs. 8f,h) associated with EM2 are weak be-

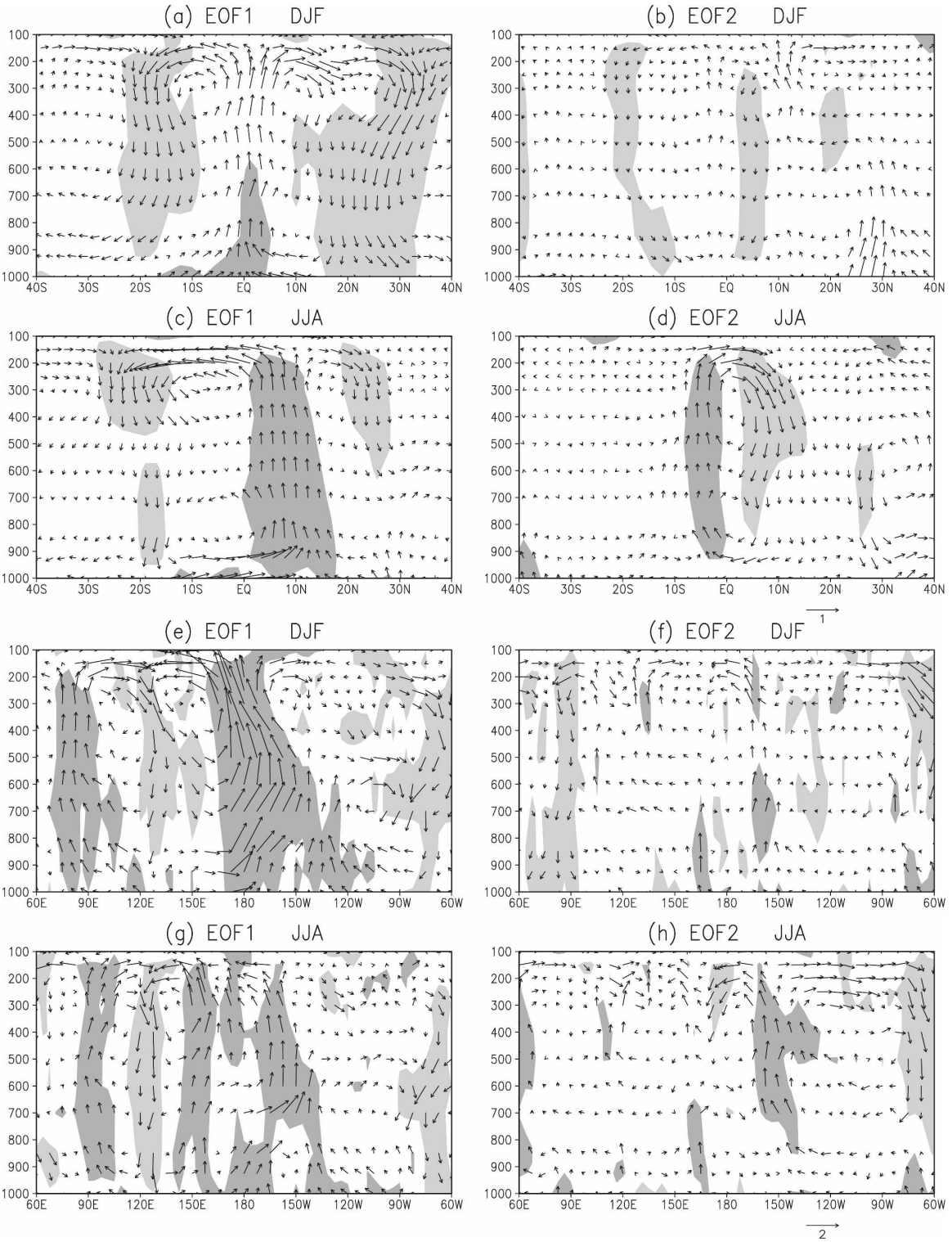

FIG. 8. As in Figs. 6 and 7, but for anomalous (a)–(d) meridional and (e)–(h) zonal circulation. Dark (light) shadings indicate anomalous updraft (downdraft) at the 1% significance level.

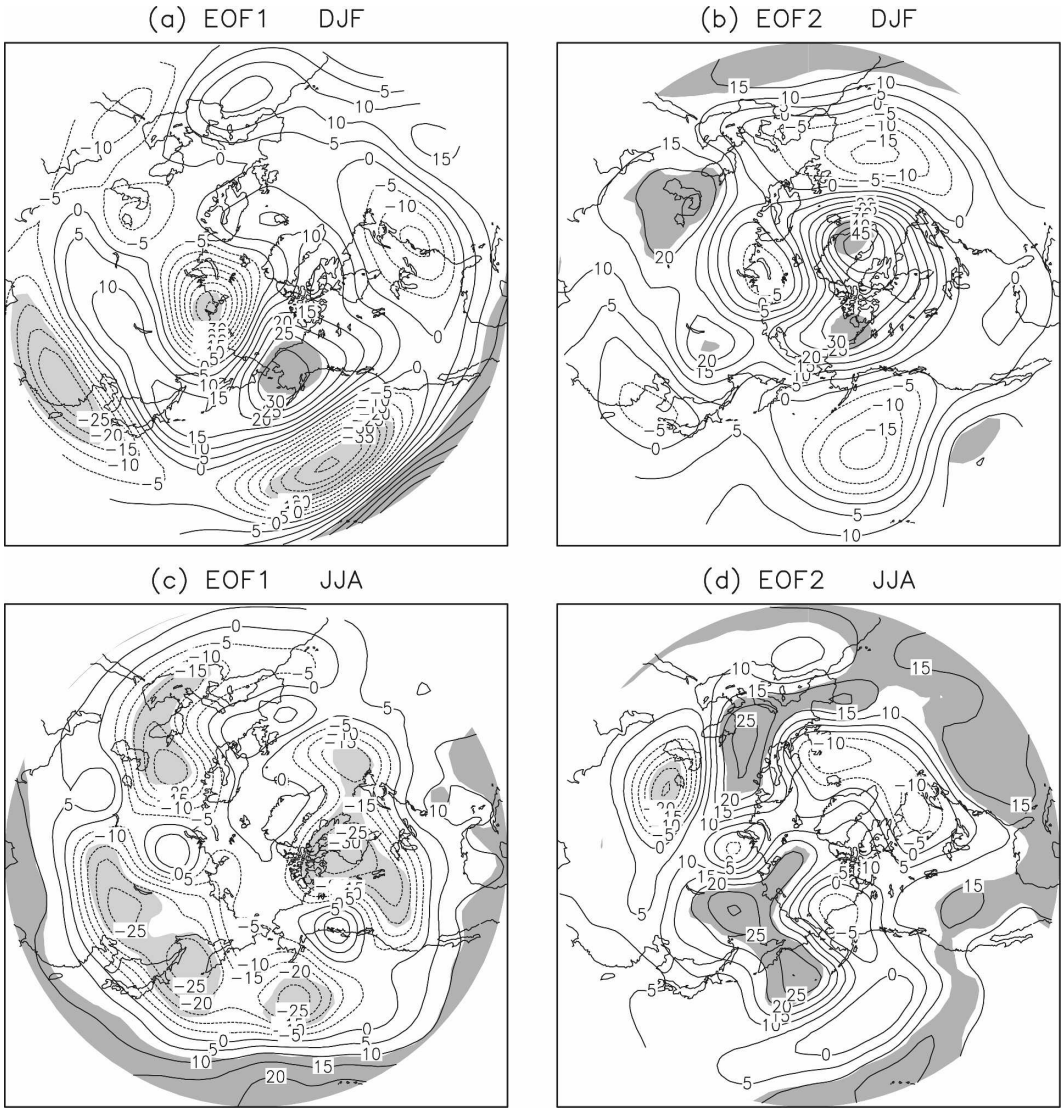

FIG. 9. 200-hPa geopotential height anomaly for (a), (b) DJF and (c), (d) JJA associated with two leading EOFs of the IPWP SST. The maps are linear regressions vs each EOF time series with a two standard deviation departure. Contour interval is 5 m and negative contours are dashed. Dark (light) shadings indicate positive (negative) height anomaly at the 1% significance level.

cause the zonal gradient of SST anomalies in EM2 is weak (Fig. 3b).

The anomalous upper-level divergent flow over the IPWP (Fig. 8) provides an important source for Rossby wave to propagate from the tropics to the extratropics (Sardeshmukh and Hoskins 1988). This type of planetary waves links anomalous convection in the IPWP to circulation anomalies in higher latitudes. The northern extratropical response to the heating and consequent divergent forcing in the IPWP region is examined in Fig. 9 by computing 200-hPa geopotential height anomalies associated with the two PC time series (Fig. 4). The anomalous DJF geopotential height field associated with the IPWP EM1 exhibits a wave train across the Asia–Arctic Ocean–Pacific–North American (PNA) regions (Fig. 9a). In the anomaly pattern associated with EM1 in DJF (Fig. 9a), there are statistically significant anomaly centers over central and eastern China, northern Russia and the Arctic, Alaska, and the central North Pacific. To some extent, this anomalous circulation pattern resembles the PNA pattern (Wallace and Gutzler 1981), which is a recurrent DJF circulation pattern especially during ENSO years (Wang and Fu 2000; Straus and Shukla 2002). However, there are additional centers of action over China, Mongolia, and Russia associated with the IPWP SST EM1. In addition

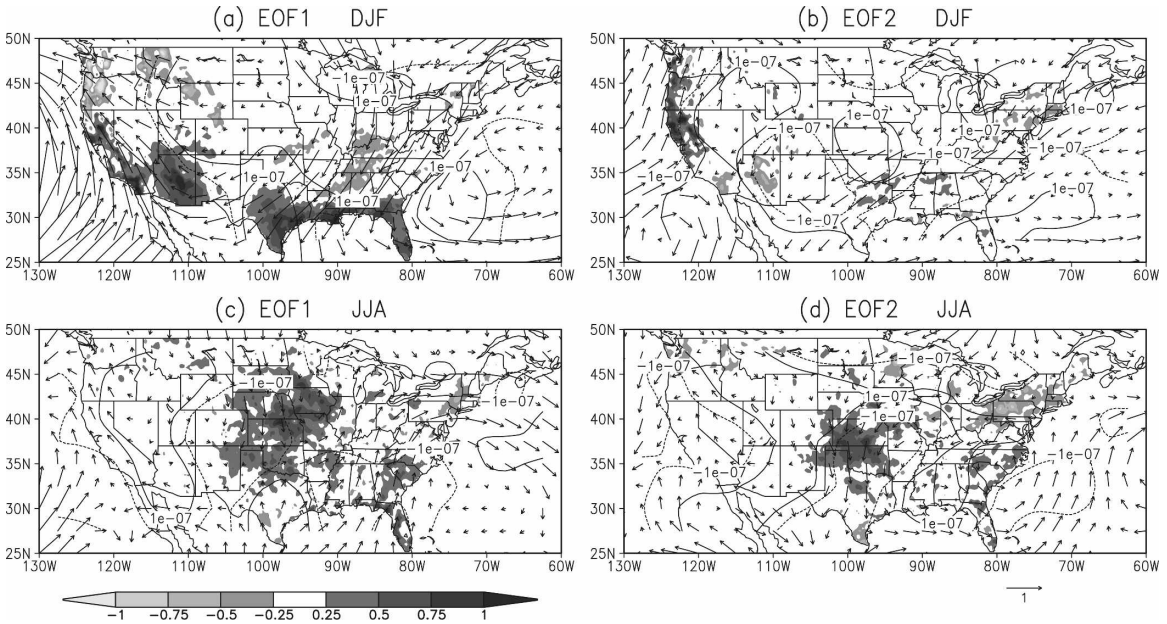

FIG. 10. As in Fig. 9, but for U.S. rainfall (unit: mm day^{-1}, shadings), 850-hPa wind (unit: m s^{-1}, vectors) and divergence (contours) anomalies. Contour value is 1×10^{-7} s^{-1} with negatives dashed and the zero contour omitted.

to its direct association with the PNA region climate variability at the decadal time scale, this anomalous 200-hPa geopotential height pattern (Fig. 9a) associated with the IPWP SST may also modulate interannual ENSO impacts on the PNA region on decadal time scales in a similar way as the Pacific decadal oscillation (PDO) does (Gershunov and Barnett 1998). In fact, there is a marginal correlation (0.31) between the PDO and EM1 when the IPWP SST leads the PDO by 1 yr but no measurable correlation (0.11) when the IPWP SST lags the PDO. The JJA 200-hPa geopotential height anomaly pattern (Fig. 9c) associated with EM1 is much more zonal and similar to the JJA North Pacific, tropical–extratropical teleconnection pattern found by Barnston and Livezey (1987). The 200-hPa geopotential height anomalies associated with EM2 in DJF (Fig. 9b) show a spatial structure similar to the Arctic Oscillation (AO; Thompson and Wallace 1998), with opposing geopotential height anomalies in northern mid- and high latitudes. Strong correlations (>0.6) between EM1 (EM2) and the 5-yr running mean PNA (AO) index are found when the IPWP SST leads the circulation indices by a decade or so. These results clearly indicate a statistically significant association between major extratropical atmospheric circulation patterns in DJF and the IPWP SSTs on the decadal time scale. The extratropical circulation anomalies in JJA (Figs. 9c,d) are relatively weaker compared to their DJF counterparts, and also display smaller-scale features, presumably due to weaker jet streams and reduced meridional absolute vorticity gradient in the northern extratropics.

Figure 10 shows DJF and JJA rainfall anomalies in the United States, associated with the decadal variation of the IPWP SST EMs, together with anomalous 850-hPa wind and divergence fields. Associated with EM1 in DJF (Fig. 10a), wetter conditions dominate the southeast coast, Arizona, and California, and drier conditions are dominant in the Pacific Northwest and middle and lower Mississippi River basin. The pattern resembles, to some degree, the typical ENSO-related seasonal-average rainfall anomalies (Ropelewski and Halpert 1986). Associated with EM2 (Fig. 10b), above-average rainfall is mainly confined to northern California and the Pacific Northwest coast. The changes in the rainfall pattern along the West Coast between the two EMs are consistent with both changes in the 850-hPa onshore flow (Figs. 10a,b) and the meridional shift of the 200-hPa cyclonic circulation near the coast (Figs. 9a,b). In JJA (Figs. 10c,d), positive rainfall anomalies are found over the northern and central Plains, which are dynamically consistent with low-level convergence in these areas. Both magnitudes of rainfall anomalies over the southern states in DJF and central Plains in JJA are approximately 1 mm day^{-1}, which is comparable or even larger than one standard deviation of interannual rainfall anomalies in DJF and JJA (Ting and Wang 1997; Wang and Ting 2000). If these rainfall anomalies in the United States are indeed caused by

decadal variability of the IPWP SSTs, these results suggest a significant impact of the IPWP decadal variability on the U.S. rainfall.

6. Ocean temperature and circulation variability associated with the IPWP decadal variability

To determine corresponding changes in oceanic circulations associated with the IPWP decadal variability, Fig. 11 shows the vertical structure of ocean temperature averaged between 2.5°S and 2.5°N, related to positive and negative phases of the two EMs of the IPWP SST, respectively. The distance between two intersections of the 28°C isotherm with the ocean surface can be taken as an approximate zonal dimension of the IPWP near the equator. Associated with EM1, DJF IPWP exhibits strong zonal variations between the two phases with an oscillation of thermocline (20°C isotherm) depth between the eastern and western Pacific (Fig. 11a). This is caused by basin-scale out-of-phase changes in temperature anomalies between the eastern and western Pacific in the 50–150-m layer, with an approximate 3°C amplitude (Fig. 11c, bottom panel), significant at the 1% level. There are also smaller but significant temperature anomalies at 100–50-m depth between the positive and negative phases of EM1 in the Indian Ocean. Associated with EM2, in contrast, there is not much zonal variation (Fig. 11b). Instead, the 28°C isotherm moves vertically between positive and negative phases, indicating significant changes in intensity (temperature) of the warm pool. The thermocline also displays coherent vertical movements between the two phases. These variations in the thermal structure are consistent with warm temperature anomalies above 100 m in the western Pacific and cold anomalies centered at 150 m in the central Pacific, and also in the Indian Ocean. In JJA, the changes in ocean temperature between the two phases in EM1 (Fig. 11c) are similar to those in DJF, with an apparent zonal variation of the warm pool in the Pacific. The out-of-phase midocean temperature anomalies in the eastern and western Pacific between the two phases in EM1 (Fig. 11c, bottom panel) are about a half of magnitudes as those in DJF (Fig. 11a, bottom panel) but significant at the 1% level. The temperature anomalies between the two phases of EM1 in the Indian Ocean are at 50–100-m depth in JJA. Similar to its DJF counterpart (Fig. 11b), the IPWP shows less zonal variation associated with EM2 in JJA (Fig. 11d). In the Indian Ocean, however, the warm pool has a much larger extension in JJA.

A similar vertical-meridional cross section for ocean temperature along 150°E longitude is shown in Fig. 12, where the IPWP has the maximum meridional extension. Unlike its zonal variation between positive and negative phases of EM1 (Figs. 11a,c), the meridional extension of the IPWP changes in an opposite way between the two phases in both DJF and JJA (Figs. 12a,c). Specifically, while the IPWP expands along the equator, it shrinks in meridional direction and vice versa. This change is accompanied by significant cooling in the tropical and subtropical western Pacific above 300-m depth, except for a narrow and shallow layer of warming above 50-m depth at the equator (Figs. 12a,c, bottom panel). There is also significant cooling between 40° and 60°N in the negative phase of EM1 when the warm pool expands in the meridional direction; this cooling is coherent from the surface to 250-m depth. Related to EM2, the warm pool also behaves differently in the meridional direction. With little change in size along the equator between the two phases (Figs. 11b,d), the warm pool exhibits large variations in its meridional size (Figs. 12b,d), especially in DJF. The changes between the two phases in EM2, however, are opposite to those in EM1 in the tropics and midlatitudes, which may thereby lead to less latitudinal variations because of a cancellation of the two EMs. Both Figs. 11 and 12 illustrate two distinctive variations of the IPWP on decadal time scales, consistent with the reconstructed annual-average warm pool based on each phase of individual EMs in Fig. 5.

To explore dynamical processes responsible for the IPWP decadal variability, Fig. 13 shows regression patterns of ocean temperature and anomalous ocean current at 7.5-m depth, associated with the two EMs. The warm pool (shaded) associated with different phases of each EM is similar to the annual-average patterns (Fig. 5), but with pronounced seasonality. The JJA warm pool has a more zonally extended north branch. The changes in size and shape of the IPWP between positive and negative phases of each EM are consistent with the results based on the vertical structure of ocean temperature in Figs. 11 and 12. Associated with EM1, the warm pool displays an out-of-phase relationship in changing zonal and meridional dimensions, indicating a strong deformation (Figs. 13a,c). In EM2, the variations between the two phases are dominated by changes in size and intensity of the warm pool (Figs. 13b,d). Associated with these temperature variations, strong anomalous surface currents are found in the equatorial Pacific and Indian Ocean and weak anomalous currents are found in the subtropics. Some of the surface current patterns may suggest an effect of thermal advection on the warm pool temperature. In the positive phase of Fig. 13a, for example, strong westerly flow in the central Pacific and easterly flow in the Indian Ocean can contribute to warming and zonal expansion of the IPWP

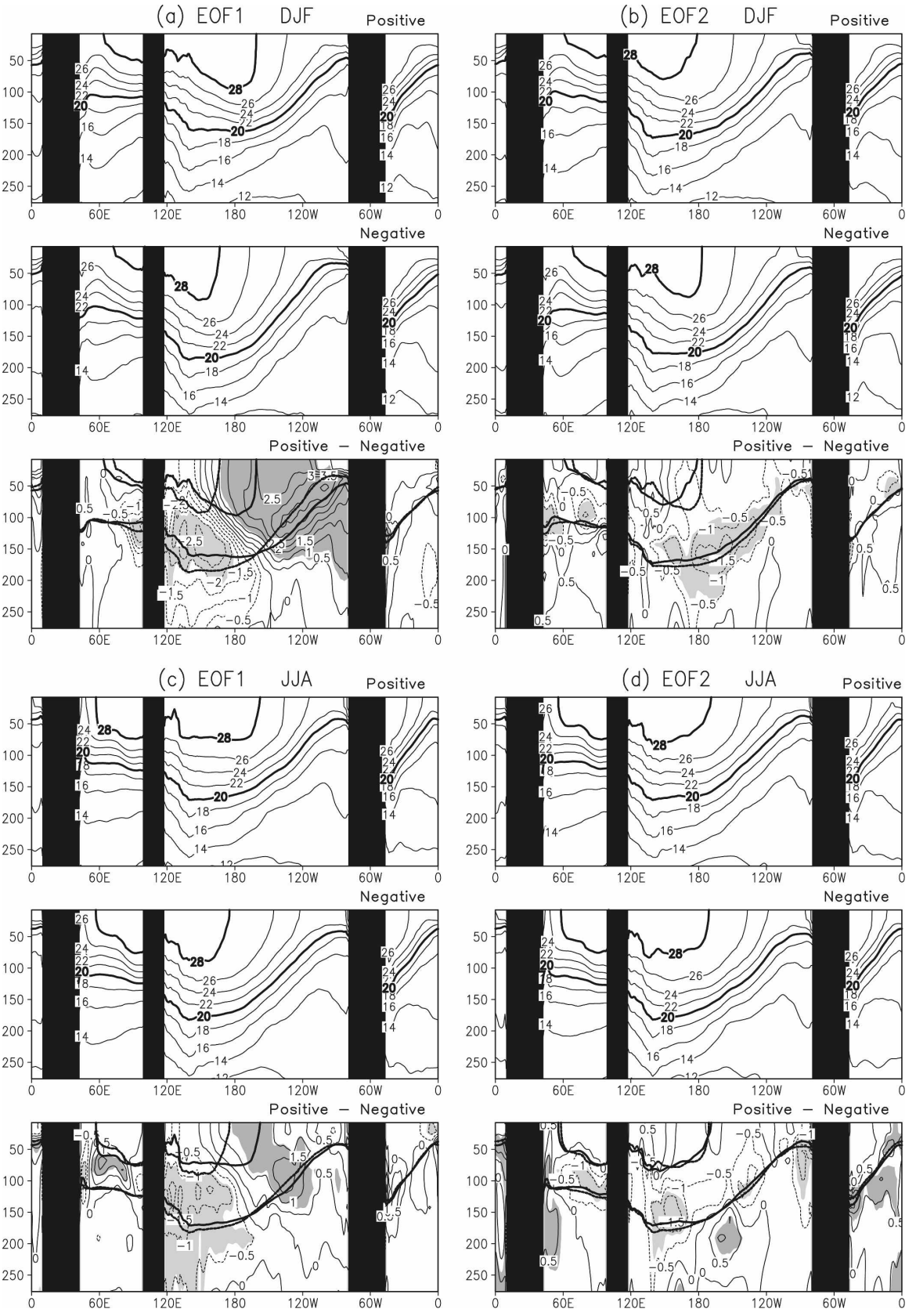

FIG. 11. As in Fig. 9, but for ocean temperature averaged over 2.5°S–2.5°N associated with (top) positive and (middle) negative phases of IPWP EOF modes, and (bottom) their differences. Contour interval is 2°C in the (top) and (middle) and 0.5°C in (bottom) with negatives dashed. Thick lines are 20° and 28°C isothermals. Shadings are same as in Fig. 9.

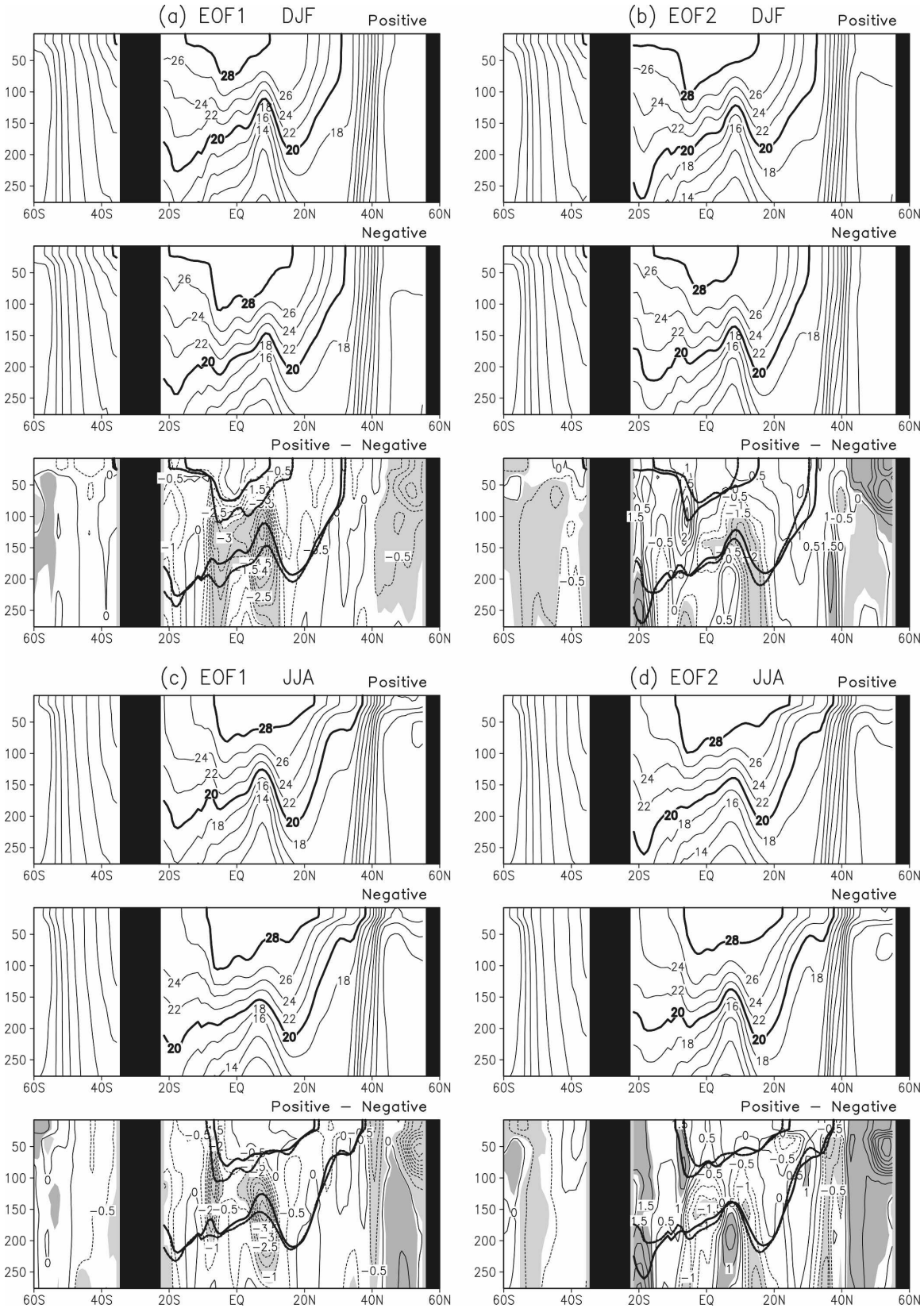

FIG. 12. As in Fig. 11, but for a latitude–depth cross section at 150°E.

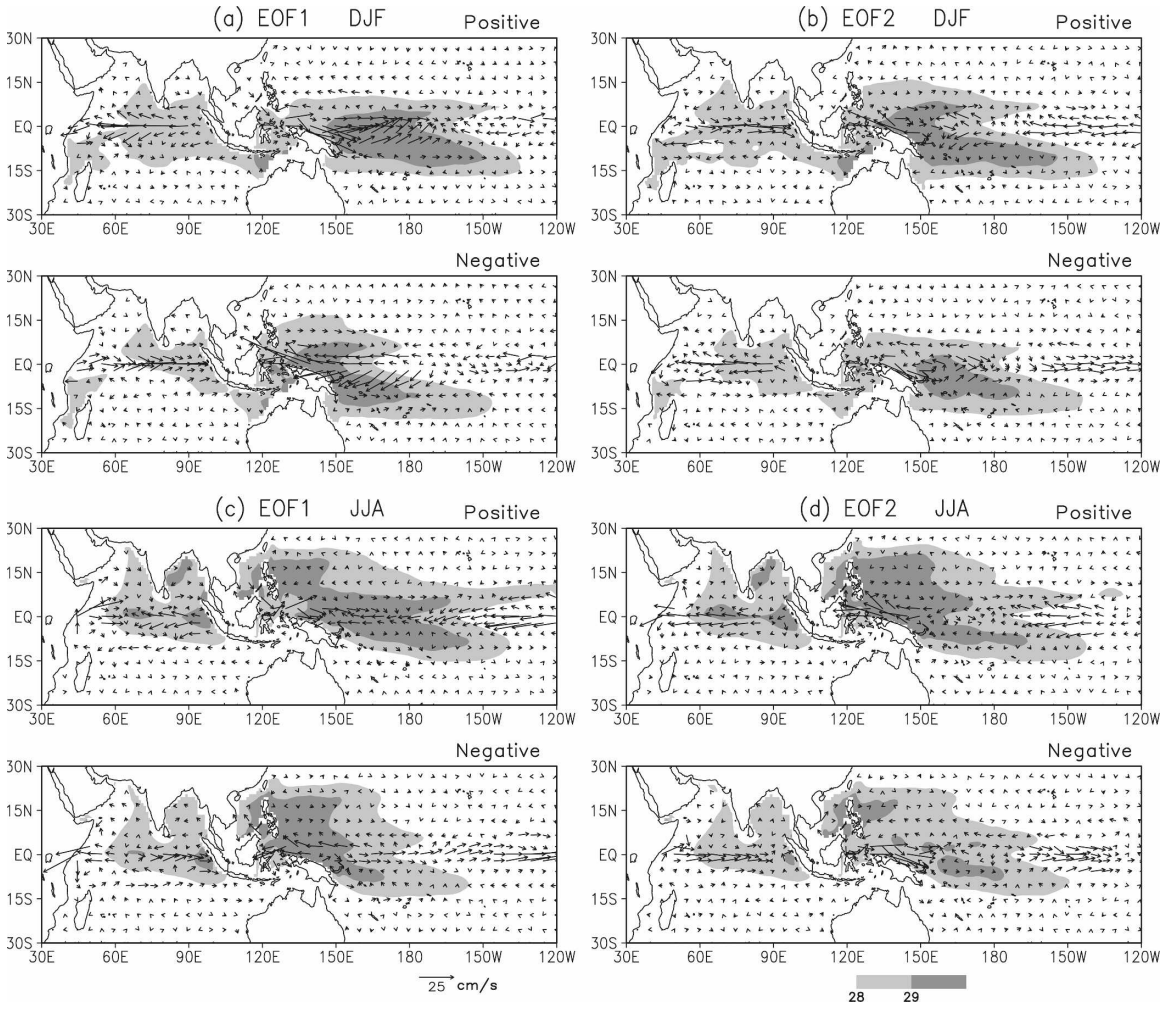

FIG. 13. As in Fig. 11, but for ocean temperature and anomalous current at 7.5-m depth. Light and dark shadings indicate temperature greater than 28° and 29°C, respectively.

through advection of mean temperature by anomalous currents. This mechanism, however, seems not to operate in JJA (Fig. 13c). Given strong horizontal temperature gradients in the extratropics (Fig. 12) and strong mean meridional currents near the surface (not shown), the exchanges between the tropics and extratropics by mean flow may also be a possible explanation of the IPWP temperature variations, as suggested by Gu and Philander (1997) for the tropical Pacific decadal variability.

Figure 14 shows a vertical cross section of anomalous meridional velocity at 150°E associated with each EM in its positive phase. Anomalous meridional currents are stronger in the Southern Hemisphere than in the Northern Hemisphere. Compared to seasonal-average meridional currents (not shown), significant meridional current anomalies associated with EM1 strengthen the Southern Hemisphere STC in both DJF and JJA, and weaken the Northern Hemisphere STC in both DJF and JJA. Meridional current anomalies associated with EM2 weaken the total STCs in both Hemispheres. Stronger STCs may lead to a stronger subduction and cooling of the ocean temperature (Mehta 1991, 1992). Since the anomalous meridional velocities are nearly opposite between the two EMs, the STCs may act differently in maintaining the two decadal EMs. Associated with EM1 in the positive phase, for example, a stronger Southern Hemisphere STC can cool the warm pool and may force it toward its negative phase. When the warm pool is in the negative phase, the anomalous meridional current in Fig. 14a changes sign and thus can weaken the total Southern Hemisphere STC that, in turn, can warm the IPWP, and can force the warm pool back to the positive phase. The changes in the strength of the STCs can be induced by subtropical surface winds (McCreary and Lu 1994; Liu 1994), such as those

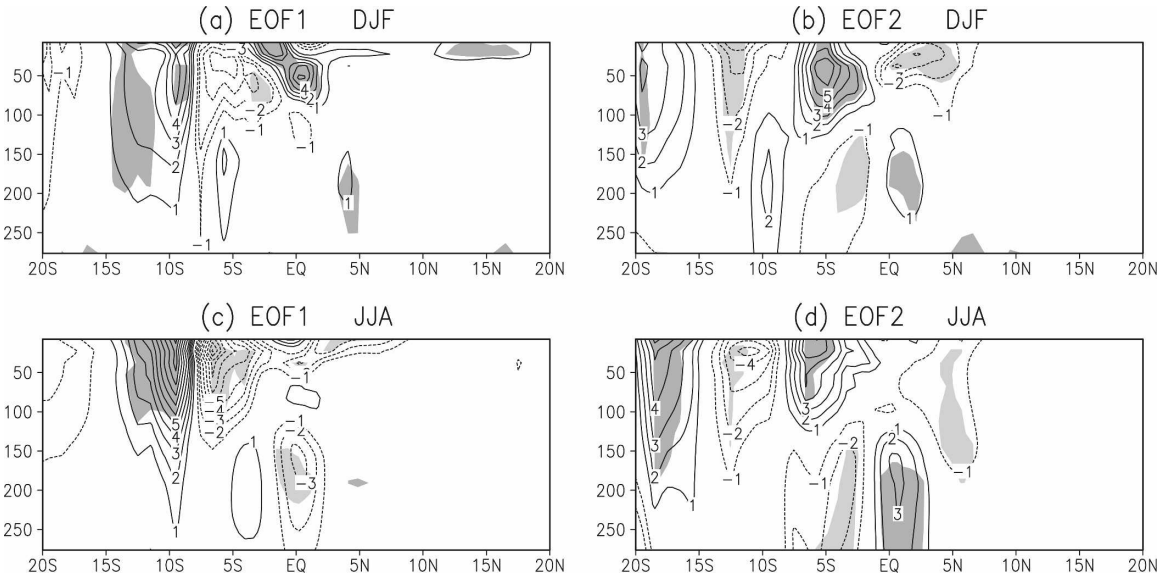

FIG. 14. As in Fig. 11, but for anomalous meridional velocity at 150°E associated with a two standard deviation departure in the positive phase of IPWP EOF time series. Contour interval is 1 cm s^{-1} with negatives dashed and zeros omitted. Dark (light) shadings indicate positive (negative) anomaly at the 1% significance level.

observed in Fig. 8 in response to the decadal IPWP SST anomalies. Therefore, the STCs, especially that in the Southern Hemisphere, can provide a negative feedback to the warm pool in EM1 and a positive feedback in EM2. Since the variations of the STCs are on a meridional advection time scale of 10–15 yr or more, which is originated from Ekman drift related equatorial upwelling, oscillations in tropical horizontal gyres, and interactions between STC pathways and other ocean currents (Schott et al. 2004; Luebbecke et al. 2008), they provide a forcing mechanism for the IPWP decadal variations. The effect of the STCs on the ENSO-like decadal mode is also suggested by Lohmann and Latif (2005) using an ocean model.

7. Conclusions

We have investigated decadal variability of the IPWP SST and its associations with variability of atmospheric and oceanic temperatures and circulations, using observed 50-yr (1952–2001) SST data, and atmospheric and oceanic reanalyses. Relative to the decadal variability of IPWP SST, there is a very strong warming trend over the 1952–2001 period of record. The decadal variability is well-described by two leading EMs of low-pass-filtered (>7 yr) SSTs. EM1 shows an ENSO-like pattern with out-of-phase SST anomalies in the western Pacific and the Indian Ocean, and EM2 shows an in-phase relationship between SSTs in these two regions. The reconstructed IPWP temperature patterns based on the two EMs show distinctive spatial evolutions. EM1 represents decadal changes in the shape of the IPWP by extending or shrinking in zonal extent and complementary changes in meridional extent. EM2 mainly represents decadal changes in intensity and size of the IPWP with less deformation.

Both atmospheric circulation, and ocean thermal and dynamic fields show consistent changes associated with the IPWP decadal variability. In general, the changes associated with EM1 are stronger than those associated with EM2. They also show strong seasonality. These decadal variations of the IPWP are associated with changes in the Hadley and Walker circulations. In addition, significant rotational flow anomalies are also found in the extratropics, presumably due to atmospheric response to divergent forcing in the IPWP region related to the decadal heating variability. We have also assessed the possible association between the IPWP decadal variability and the U.S. rainfall. Consistent with the upper-level flow anomalies and 850-hPa convergence–divergence patterns associated with the two EMs are rainfall anomalies over the United States. In DJF, the rainfall anomalies are mainly in Florida, the Gulf Coast, southern Texas, Arizona, and along the West Coast; and in JJA, the rainfall anomalies are mainly in the Midwest and the Southeast. Since these rainfall anomalies are a significant fraction of seasonal-average rainfall and since these anomalies persist for many years, they potentially make a significant impact on U.S. water resources and agriculture.

Analyses of ocean temperature and currents based on the two EMs indicate that several physical processes suggested in previous studies of tropical decadal variability may also be involved in the IPWP decadal variations. They include advections of mean upper-ocean temperature by both mean and anomalous ocean currents and effects of the STCs on the IPWP decadal SST anomalies. Results based on the ocean thermodynamical fields suggest the existence of feedbacks between the IPWP decadal SST and the STCs. A speculative negative feedback loop picture consistent with EM1 and associated atmospheric and oceanic anomalies is as follows. Warmer decadal SST anomalies in the IPWP region intensify the Hadley circulation and associated surface wind anomalies in the subtropics, which, in turn, strengthen the wind-driven STCs. Stronger STCs induce a stronger subduction and cool the warm pool. Given the fact that the changes in STCs are on decadal time scales, the above processes provide a negative feedback between IPWP SST and the STCs to the decadal oscillation of the warm pool SST. Similarly, a positive feedback loop between warm pool SST and the STCs is suggested by EM2 and associated atmospheric and oceanic anomalies.

Although the results of this exploratory study are exciting and possibly very important for climate prediction at multiyear to decadal time scales, the results must be considered suggestive. Further observational, modeling, and reanalysis studies are necessary to understand physics of the IPWP decadal variability and its impacts on global climate, and assess their predictability. While the apparent physical consistency between SST EMs and anomalous Hadley and Walker circulations is encouraging, further research with atmospheric models and reanalysis systems is necessary to quantify the IPWP SST EMs' impacts on global atmospheric circulations. Observed SSTs are specified as a lower boundary condition and actual observations of winds and temperatures are assimilated in the NCEP–NCAR reanalyses model. The former may produce anomalous, thermally direct atmospheric circulations in response to SST anomalies in the reanalysis model even in the absence of any such signals in atmospheric observations. Therefore, multiple realizations of the atmospheric climate record should be produced by using various combinations of observed boundary conditions and observed atmospheric data. Similarly, there is apparent physical consistency between the IPWP SST variability and variability of subsurface temperatures and surface currents produced by the SODA reanalysis system. In view of SODA's limitations described in section 2, however, long records of assimilated ocean data should be produced either with a more accurate formulation of SODA or with another ocean data reanalysis system so that statistical characteristics of the IPWP decadal variability can be quantified as well as a more reliable insight into the physics of the variability can be derived. Also, realizations of atmospheric and oceanic climate records should be produced with "frozen" observing systems to see impacts of changing observing systems on analysis of decadal climate variability. Last, but most importantly, as mentioned in section 2, oceanic observations in the IPWP region before the 1980s were sparse in their spatial and temporal coverage, and the accuracy of SST and subsurface ocean observations was unknown. In view of the suggestive but potentially very important results of this and other studies, continuous time series of high-quality, in situ and remote sensing–based ocean observations should be maintained in the IPWP region.

Acknowledgments. This research was partially supported by NASA Grant NNG05GQ08G and NOAA Grant NA03OAR4310152. The authors are thankful to Dr. Eric Lindstrom for his encouragement to undertake this study and two anonymous reviewers for their insightful and constructive comments and suggestions. The NOAA ERSST V2 data and CPC U.S. rainfall data are provided by the NOAA/OAR/ESRL PSD, Boulder, Colorado, from their Web site at http://www.cdc.noaa.gov.

REFERENCES

Ashok, K., W.-L. Chan, T. Motoi, and T. Yamagata, 2004: Decadal variability of the Indian Ocean dipole. *Geophys. Res. Lett.,* **31,** L24207, doi:10.1029/2004GL021345.

Barnston, A. G., and R. E. Livezey, 1987: Classification, seasonality, and persistence of low frequency atmospheric circulation patterns. *Mon. Wea. Rev.,* **115,** 1083–1126.

Brijker, J. M., S. J. A. Jung, G. M. Ganssen, T. Bickert, and D. Kroon, 2007: ENSO related decadal scale climate variability from the Indo-Pacific warm pool. *Earth Planet. Sci. Lett.,* **253,** 67–82.

Carton, J. A., G. Chepurin, X. Cao, and B. S. Giese, 2000: A Simple Ocean Data Assimilation analysis of the global upper ocean 1950–95. Part I: Methodology. *J. Phys. Oceanogr.,* **30,** 294–309.

Chelliah, M., and G. D. Bell, 2004: Tropical multidecadal and interannual climate variability in the NCEP–NCAR reanalysis. *J. Climate,* **17,** 1777–1803.

Chen, G., C. Y. Fang, C. Y. Zhang, and Y. Chen, 2004: Observing the coupling effect between warm pool and "rain pool" in the Pacific Ocean. *Remote Sens. Environ.,* **91,** 153–159.

Clarke, A. J., J. Wang, and S. Van Gorder, 2000: A simple warm-pool displacement ENSO model. *J. Phys. Oceanogr.,* **30,** 1679–1691.

Clement, A. C., R. Seager, and R. Murtugudde, 2005: Why are there tropical warm pools? *J. Climate,* **18,** 5294–5311.

D'Arrigo, R., and Coauthors, 2006: The reconstructed Indonesian warm pool sea surface temperatures from tree rings and cor-

als: Linkages to Asian monsoon drought and El Niño–Southern Oscillation. *Paleoceanography,* **21,** PA3005, doi:10.1029/2005PA001256.

Duchon, C. E., 1979: Lanczos filter in one and two dimensions. *J. Appl. Meteor.,* **18,** 1016–1022.

Fasullo, J., and P. Webster, 1999: Warm pool SST variability in relation to the surface energy balance. *J. Climate,* **12,** 1292–1305.

Fu, R., A. D. Del Genio, and W. B. Rossow, 1994: Influence of ocean surface conditions on atmospheric vertical thermodynamic structure and deep convection. *J. Climate,* **7,** 1092–1108.

Fukumori, I., 2006: What is data assimilation really solving, and how is the calculation actually done? *Ocean Weather Forecasting: An Integrated View of Oceanography,* E. P. Chasignet and J. Verron, Eds., Springer, 317–339.

Gershunov, A., and T. P. Barnett, 1998: Interdecadal modulation of ENSO teleconnections. *Bull. Amer. Meteor. Soc.,* **79,** 2715–2725.

Godfrey, J. S., and E. J. Lindstrom, 1989: The heat budget of the equatorial western Pacific surface mixed layer. *J. Geophys. Res.,* **94,** 8007–8017.

Graham, N. E., 1994: Decadal-scale climate variability in the tropical and North Pacific during the 1970s and 1980s: Observations and model results. *Climate Dyn.,* **10,** 135–162.

——, and T. P. Barnett, 1987: Observations of sea surface temperature and convection over tropical oceans. *Science,* **238,** 657–659.

Gu, D., and S. G. H. Philander, 1997: Interdecadal climate fluctuations that depend on exchanges between the tropics and extratropics. *Science,* **275,** 805–807.

Higgins, R. W., W. Shi, E. Yarosh, and R. Joyce, 2000: *Improved United States Precipitation Quality Control System and Analysis.* NCEP/CPC Atlas No. 7. [Available online at http://www.cpc.noaa.gov/index.php.]

Huang, B., and V. M. Mehta, 2004: The response of the Indo-Pacific Warm Pool to interannual variations in net atmospheric freshwater. *J. Geophys. Res.,* **109,** C06022, doi:10.1029/2003JC002114.

——, and ——, 2005: The response of the Pacific and Atlantic Oceans to interannual variations in net atmospheric freshwater. *J. Geophys. Res.,* **110,** C08008, doi:10.1029/2004JC002830.

Kalnay, E., and Coauthors, 1996: The NCEP/NCAR 40-Year Reanalysis Project. *Bull. Amer. Meteor. Soc.,* **77,** 437–471.

Kistler, R., and Coauthors, 2001: The NCEP–NCAR 50-Year Reanalysis: Monthly means CD-ROM and documentation. *Bull. Amer. Meteor. Soc.,* **82,** 247–267.

Lindstrom, E., R. Lukas, R. Fine, E. Firing, S. Godfrey, G. Meyers, and M. Tsuchiya, 1987: The western equatorial Pacific Ocean circulation study. *Nature,* **330,** 533–537.

Liu, Z., 1994: A simple model of the mass exchange between the subtropical and tropical ocean. *J. Phys. Oceanogr.,* **24,** 1153–1165.

Lohmann, K., and M. Latif, 2005: Tropical Pacific decadal variability and the subtropical–tropical cells. *J. Climate,* **18,** 5163–5178.

Luebbecke, J. F., C. W. Boening, and A. Biastoch, 2008: Variability in the subtropical–tropical cells and its effect on near-surface temperature of the equatorial Pacific: A model study. *Ocean Sci.,* **4,** 73–88.

Lukas, R., and E. Lindstrom, 1991: The mixed layer of the western equatorial Pacific Ocean. *J. Geophys. Res.,* **96,** 3343–3357.

Matsuura, T., and S. Iizuka, 2000: Zonal migration of the Pacific warm-pool tongue during El Niño events. *J. Phys. Oceanogr.,* **30,** 1582–1600.

McCreary, J., and P. Lu, 1994: Interaction between the subtropical and equatorial ocean circulation: The subtropical cell. *J. Phys. Oceanogr.,* **24,** 466–497.

Mehta, V. M., 1991: Meridional oscillations in an idealized ocean–atmosphere system. Part I: Uncoupled modes. *Climate Dyn.,* **6,** 49–65.

——, 1992: Meridionally propagating interannual-to-interdecadal variability in a linear ocean–atmosphere model. *J. Climate,* **5,** 330–342.

——, and C. Fayos, 2005: Decadal variability of El Niño events in the northern hemisphere winter and its impacts on the global climate. *Workshop on Decadal Climate Variability,* Warrenton, VA, CRCES.

Neale, R., and J. Slingo, 2003: The maritime continent and its role in the global climate: A GCM study. *J. Climate,* **16,** 834–848.

North, G. R., T. L. Bell, R. F. Cahalan, and F. J. Moeng, 1982: Sampling errors in the estimation of empirical orthogonal functions. *Mon. Wea. Rev.,* **110,** 699–706.

Picaut, J., M. Ioualalen, C. Menkes, T. Delcroix, and M. J. McPhaden, 1996: Mechanism of the zonal displacements of the Pacific warm pool: Implications for ENSO. *Science,* **274,** 1486–1489.

Ramanathan, V., and W. Collins, 1991: Thermodynamic regulation of ocean warming by cirrus clouds deduced from observations of the 1987 El Niño. *Nature,* **351,** 27–32.

——, B. Subasilar, G. J. Zhang, W. Conant, R. D. Cess, J. T. Kiehi, H. Grassi, and L. Shi, 1995: Warm pool heat budget and shortwave cloud forcing: A missing physics? *Science,* **267,** 499–503.

Ropelewski, C. F., and M. S. Halpert, 1986: North American precipitation and temperature patterns associated with the El Niño–Southern Oscillation (ENSO). *Mon. Wea. Rev.,* **114,** 2352–2362.

Sardeshmukh, P. D., and B. J. Hoskins, 1988: The generation of global rotational flow by steady idealized tropical divergence. *J. Atmos. Sci.,* **45,** 1228–1251.

Schneider, N., T. Barnett, M. Latif, and T. Stockdale, 1996: Warm pool physics in a coupled GCM. *J. Climate,* **9,** 219–239.

Schoenefeldt, R., and F. A. Schott, 2006: Decadal variability of the Indian Ocean cross-equatorial exchange in SODA. *Geophys. Res. Lett.,* **33,** L08602, doi:10.1029/2006GL025891.

Schott, F. A., M. Dengler, and R. Schoenefeldt, 2002: The shallow overturning circulation of the Indian Ocean. *Prog. Oceanogr.,* **52,** 57–103.

——, J. P. McCreary, and G. C. Johnson, 2004: Shallow overturning circulation of the tropical-subtropical oceans. *Earth's Climate: The Ocean-Atmosphere Interaction, Geophys. Monogr.,* Amer. Geophys. Union, Vol. 147, 261–304.

Smith, T. M., and R. W. Reynolds, 2004: Improved extended reconstruction of SST (1854–1997). *J. Climate,* **17,** 2466–2477.

Solomon, A., and F.-F. Jin, 2005: A study of the impact of off-equatorial warm pool SST anomalies on ENSO cycles. *J. Climate,* **18,** 274–286.

Solomon, S., D. Qin, M. Manning, M. Marquis, K. Averyt, M. M. B. Tignor, H. L. Miller Jr., and Z. Chen, Eds., 2007: *Climate Change 2007: The Physical Sciences Basis.* Cambridge University Press, 1009 pp.

Straus, D. M., and J. Shukla, 2002: Does ENSO force the PNA? *J. Climate,* **15,** 2340–2358.

Thompson, D. W. J., and J. M. Wallace, 1998: The Arctic Oscil-

lation signature in the wintertime geopotential height and temperature fields. *Geophys. Res. Lett.,* **25,** 1297–1300.

Tian, B., G. Zhang, and V. Ramanathan, 2001: Heat balance in the Pacific warm pool atmosphere during TOGA COARE and CEPEX. *J. Climate,* **14,** 1881–1893.

Ting, M., and H. Wang, 1997: Summertime U.S. precipitation variability and its relation to Pacific sea surface temperature. *J. Climate,* **10,** 1853–1873.

Trenberth, K., and J. Hurrell, 1994: Decadal atmosphere–ocean variations in the Pacific. *Climate Dyn.,* **9,** 303–319.

Waliser, D. E., and N. E. Graham, 1993: Convective cloud systems and warm pool SSTs: Coupled interactions and self-regulation. *J. Geophys. Res.,* **98,** 12 881–12 893.

Wallace, J. M., and D. S. Gutzler, 1981: Teleconnections in the geopotential height field during the Northern Hemisphere winter. *Mon. Wea. Rev.,* **109,** 784–812.

Wang, B., and X. Xie, 1998: Coupled modes of the warm pool climate system. Part I: The role of air–sea interaction in maintaining Madden–Julian oscillation. *J. Climate,* **11,** 2116–2135.

Wang, H., and R. Fu, 2000: Winter monthly mean atmospheric anomalies over the North Pacific and North America associated with El Niño SSTs. *J. Climate,* **13,** 3435–3447.

——, and M. Ting, 2000: Covariabilities of winter U.S. precipitation and Pacific sea surface temperatures. *J. Climate,* **13,** 3711–3719.

Xie, S.-P., H. Annamalai, F. Schott, and J. P. McCreary Jr., 2002: Origin and predictability of South Indian Ocean climate variability. *J. Climate,* **15,** 864–874.

Yeh, S.-W., and B. P. Kirtman, 2004: Tropical Pacific decadal variability and ENSO amplitude modulation in a CGCM. *J. Geophys. Res.,* **109,** C11009, doi:10.1029/2004JC002442.

Zhang, D., and M. J. McPhaden, 2006: Decadal variability of the shallow Pacific meridional overturning circulation: Relation to tropical sea surface temperatures in observations and climate change models. *Ocean Modell.,* **15,** 250–273.

Zhang, Y., J. M. Wallace, and D. S. Battisti, 1997: ENSO-like interdecadal variability: 1900–93. *J. Climate,* **10,** 1004–1020.